J Appl Electrochem (2014) 44:455–465
DOI 10.1007/s10800-013-0646-y

RESEARCH ARTICLE

Electrodeposition and characterization of nickel–copper metallic foams for application as electrodes for supercapacitors

S. Eugénio · T. M. Silva · M. J. Carmezim · R. G. Duarte · M. F. Montemor

Received: 26 July 2013 / Accepted: 18 November 2013 / Published online: 29 November 2013

Abstract Nickel–copper metallic foams were electrodeposited from an acidic electrolyte, using hydrogen bubble evolution as a dynamic template. Their morphology and chemical composition was studied by scanning electron microscopy and related to the deposition parameters (applied current density and deposition time). For high currents densities (above 1 A cm^{-2}) the nickel–copper deposits have a three-dimensional foam-like morphology with randomly distributed nearly-circular pores whose walls present an open dendritic structure. The nickel–copper foams are crystalline and composed of pure nickel and a copper-rich phase containing nickel in solid solution. The electrochemical behaviour of the material was studied by cyclic voltammetry and chronopotentiometry (charge–discharge curves) aiming at its application as a positive electrode for supercapacitors. Cyclic voltammograms showed that the Ni–Cu foams have a pseudocapacitive behaviour. The specific capacitance was calculated from charge–discharge data and the best value (105 F g^{-1} at 1 mA cm^{-2}) was obtained for nickel–copper foams deposited at 1.8 A cm^{-2} for 180 s. Cycling stability of these foams was also assessed and they present a 90 % capacitance retention after 10,000 cycles at 10 mA cm^{-2}.

Keywords Nickel–copper · Nanostructured foams · Electrodeposition · Electrodes for supercapacitors

S. Eugénio (✉) · T. M. Silva · M. J. Carmezim · R. G. Duarte · M. F. Montemor
ICEMS, Instituto Superior Técnico, University of Lisbon, Av. Rovisco Pais, 1049-001 Lisbon, Portugal
e-mail: s.eugenio@ist.utl.pt

T. M. Silva
Department of Mechanical Engineering, Instituto Superior de Engenharia de Lisboa, 1950-062 Lisbon, Portugal

M. J. Carmezim
ESTSetúbal, Instituto Politécnico de Setúbal, 2910-761 Setúbal, Portugal

R. G. Duarte
ESTBarreiro, Instituto Politécnico de Setúbal, 2839-001 Barreiro, Portugal

M. F. Montemor
Department of Chemical Engineering, Instituto Superior Técnico, University of Lisbon, Av. Rovisco Pais, 1049-001 Lisbon, Portugal

1 Introduction

Nanoporous architectures have become highly interesting morphologies sought for applications where high specific area is an important requirement such as catalysis and energy storage devices [1, 2]. In the latter field, electrochemical supercapacitors have attracted great attention due to their ability to stand a very large number of charge and discharge cycles, increased power density and increased lifetime. However, and comparatively to batteries, these devices still lack energy density. In order to overcome this drawback it is necessary to develop new electrode materials with optimal properties. Pseudocapacitive materials, such as transition metal oxides/hydroxides, have been explored for this application due to their high theoretical capacitances (several times larger than those of carbonaceous materials) and multiple oxidation states [1]. Despite numerous research efforts, these materials often present insufficient capacitance and poor cycling stability mostly due to the incomplete reversibility of some electrochemical reactions and the development of a resistive response over time.

Nanoporous metallic foams (NMFs) are typically 3D structures of interconnected pores with nano-ramified walls that usually exhibit porosities above 50 %, and a wide pore size distribution. These structures allow the fast diffusion of actives species through the material and provide an increased surface area for electrochemical reactions, which are of paramount importance in electrodes for supercapacitors. Furthermore, they combine these properties with those characteristic of metals, such as good electrical and thermal conductivity and ductility/malleability.

There are several methods for the fabrication of metallic highly porous networks, such as dealloying and hard template-based synthesis [2, 3]. Dealloying consists on the selective dissolution of one of the metals of a metallic alloy resulting in the formation of a nanoporous morphology [3]. In hard-template synthesis, the metal is deposited, by chemical or electrochemical route, in the voids of the template which is then removed by chemical dissolution or burning [2]. Another versatile technique for the production of porous materials is electrodeposition that can originate a large array of morphologies by tuning of process parameters [2, 4]. In particular, by taking advantage of the dynamic template formed by hydrogen bubbling that often occurs simultaneously with metal deposition, this process becomes a one-step, low-cost method for the fabrication of NMFs [5, 6]. Furthermore, electrodeposited NMFs are typically formed on metallic substrates of high electronic conductivity, which constitutes an advantage for fabrication of supercapacitor electrodes since the active material is directly applied on the current collector.

The concept was first established by Shin and Liu [6] Shin et al. [7] that showed that self-supported metallic foams of copper and tin, with a nano-ramified dendritic structure, could be deposited on copper substrates from an acidic electrolyte by application of a high cathodic current. The phenomenology of copper foams formation by hydrogen bubble templating has been thoroughly studied by Nikolić [8], Nikolić et al. [9]. The morphology of copper foams is closely related to the nucleation and evolution of hydrogen bubbles during deposition. It is generally accepted that hydrogen bubbles first form on the substrate preventing the deposition of copper in those sites [5–9]. The continuous gas evolution disrupts the direct diffusion of metal ions to the electrode and forces metal growth to occur between the gas bubbles (assuming that the metal growth is diffusion controlled). In this way, hydrogen bubbles act as a negative dynamic template around which metal grows, thus forming a foam structure.

The structure of the porous metal foam formed by this process depends closely on the deposition parameters and electrolyte composition. The pore size of copper foams can be decreased (and pore density increased) by decreasing copper concentration or increasing H_2SO_4 concentration in solution, given that both parameters enhance hydrogen evolution [6–8]. On the other hand, longer deposition time, leads to bigger pore size due to the growth of hydrogen bubbles overtime and coalescence of adjacent bubbles [6, 7]. Porosity can also be controlled by additives in the electrolyte that may act as bubble stabilizers and suppress bubble coalescence or have catalytic effect on the Cu deposition [10, 11].

As stated previously, copper NMFs have been the most studied materials but NMFs of tin [7], silver [12], palladium [13] and gold [14] have also been fabricated by electrodeposition using the dynamic hydrogen template method. On the other hand, few papers have discussed the fabrication of NMFs containing transition metals such as nickel and cobalt, which have an increased importance as low-cost alternatives to noble metals for high reactive surface applications. Recently, Choi et al. [15] reported the fabrication of nickel NMFs by electrodeposition of nickel–copper NMFs on copper-coated alumina and subsequent electrochemical etching of copper. As for pure copper foams, the deposits show a foam-like structure with nano-ramified walls.

In the present work, nickel–copper highly porous metallic foams were electrodeposited on stainless steel substrates using the dynamic hydrogen bubble template for application as electrodes for supercapacitors. Stainless steel was chosen because it is suitable material for current collectors due to its relative low cost, good conductivity and high corrosion resistance. The work focus on the effect of the applied current and deposition time on the morphology and composition of the metallic foams and studies their electrochemical behaviour in alkaline solution aiming at their application as positive electrodes for supercapacitors.

2 Methods

Nickel–copper foams were electrodeposited from an electrolyte solution containing 0.5 M $NiSO_4{\cdot}7H_2O$, 1.5 M H_2SO_4, 1 M HCl and 0.01 M $CuSO_4{\cdot}5H_2O$. Analytical grade chemicals were used in solutions preparation.

All electrodeposition experiments were carried out at room temperature in a 2-electrode cell connected to a power source (Kikusui Electronics, Model PAB 32-3). The working electrode was a stainless steel plate with an active area of 1.65 cm^2 and a platinum plate was used as counter electrode. Prior to deposition, the stainless steels substrates were polished with a 1,000 SiC grit paper, cleaned with acetone in ultrasound and dried with a jet of cold air. Electrodeposition was carried out in galvanostatic mode by applying current densities between 0.6 and 1.8 A cm^{-2}. The deposition time was changed between 30 and 180 s.

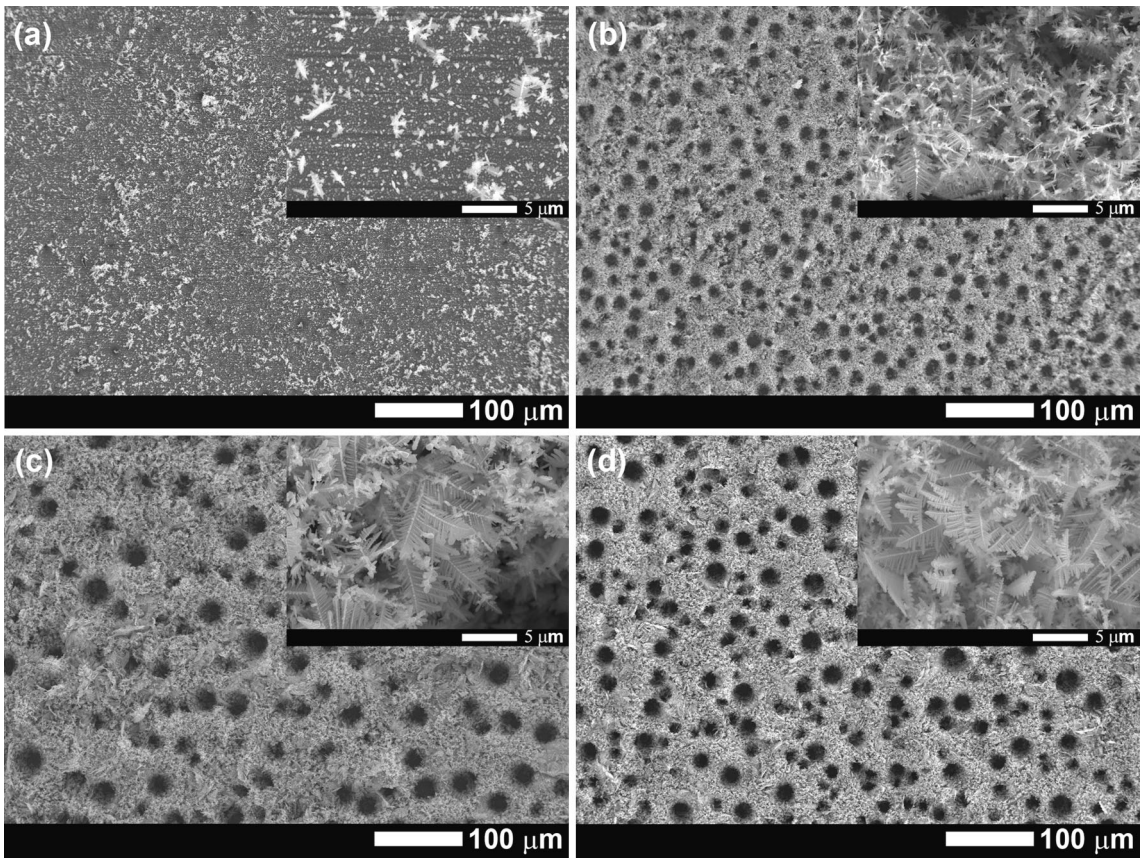

Fig. 1 SEM images of Ni–Cu foams deposited for 90 s at **a** 0.5, **b** 1, **c** 1.5 and **d** 1.8 A cm^{-2} on stainless steel. Images insets show higher magnifications

Electrodeposition at 0.6, 1, 1.5 and 1.8 A cm^{-2} for 90 s that resulted in films with 0.8 ± 0.3, 1.7 ± 0.2, 2.9 ± 0.3 and 4 ± 0.3 mg respectively. Films deposited at 1.8 A cm^{-2} for 30, 60, 90 and 180 s had masses of 0.8 ± 0.3, 2.1 ± 0.7, 4.1 ± 0.8, 6.1 ± 0.3, 10.2 ± 0.3 mg respectively.

Surface morphology and chemical composition of the metallic foams were characterised by scanning electron microscopy (SEM, Hitachi S2400) and energy dispersive X-ray spectroscopy (EDS, Rontec standard detector), respectively.

The crystallographic structure of the films was studied by X-ray diffraction (XRD) using a Bruker D8 Advance diffractometer with a Bragg–Brentano geometry working with Cu radiation (0.154056 nm). Phase identification is performed by the Hanawalt method [16], comparing the position of the three most intense peaks in the diffractogram with known diffractograms of pure substances referred in the ICCDD database.

The electrochemical performance of Ni–Cu foams was assessed by cyclic voltammetry and chronopotentiometry using a 3-electrode cell configuration connected to a Voltalab PGZ 100 potentiostat. The metallic foam was used as the working electrode, a platinum plate as counter electrode and a saturated calomel electrode (SCE) as reference. All measurements were carried out in 1 M KOH electrolyte at room temperature.

3 Results and discussion

The typical morphology of films obtained by electrodeposition at current densities between 0.6 and 1.8 A cm^{-2} are presented in Fig. 1. The application of a current density of 0.6 A cm^{-2} (Fig. 1a) fails to produce three-dimensional structures. In these conditions, smooth films composed of angular grains, with randomly distributed isolated dendrites, are formed and the topography of the underlying substrate, resulting from polishing, is still visible. When the applied current density increases up to 1 A cm^{-2} or above (Fig. 1b–d), the resulting films present a foam-like morphology with randomly distributed nearly-circular pores, whose walls present an open dendritic structure. Also, for higher current densities, the dendrites become larger and more ramified, as can be seen in the high magnification insets of Fig. 1.

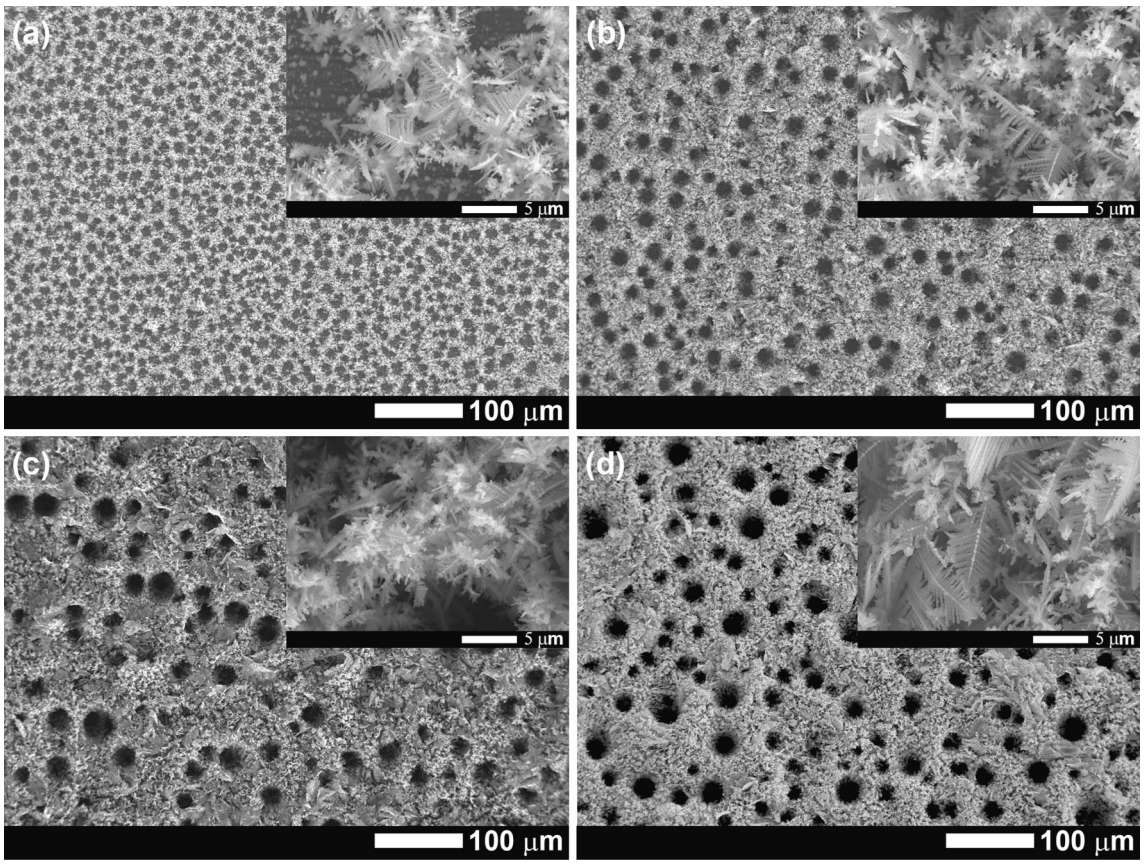

Fig. 2 SEM images of Ni–Cu foams deposited at 1.8 A cm^{-2} for **a** 30, **b** 60, **c** 120 and **d** 180 s. Images insets show higher magnifications

Figure 2 shows the typical morphology of Ni–Cu films deposited at 1.8 A cm^{-2} and its variation with the deposition time. For a deposition time of 30 s (Fig. 2a), intertwined dendrites are formed around circular areas of the substrate, where a continuous film composed of angular grains is visible. As the deposition time increases (Figs. 1d, 2b–d), a three-dimensional foam-type film is formed, showing randomly distributed pores. The interconnected dendritic structure of the pore walls is maintained, even for the longest deposition times (inset of Fig. 2d). At the surface of the film, dendrites do not present any preferential growth direction (in relation to the substrate), being randomly oriented. As the deposition time increases, dendrites assume a fern-like structure with secondary and tertiary branching (inset of Fig. 2c, d) maintaining a non-compact pore wall. Hence, the porosity of the metallic foams arises not only from the existence of pores but also from to the empty space in pore walls due to the open dendritic structure.

Figure 3 shows the variation of surface pore area and density with the deposition time. The surface pore size in the Ni–Cu foams increases with the deposition time and simultaneously, the density of surface pores decreases, in accordance with the morphologies depicted in Fig. 2.

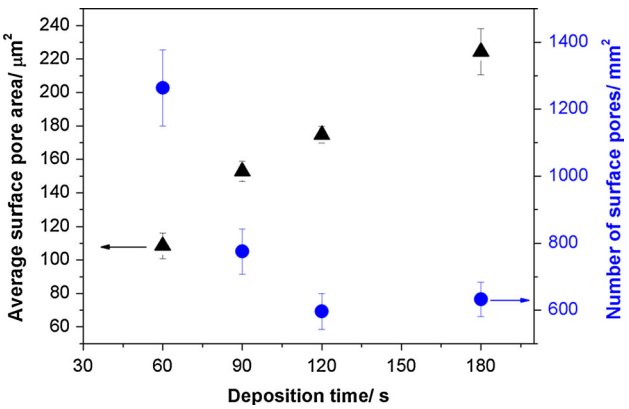

Fig. 3 Variation of surface pore area and number of surface pores with deposition time of Ni–Cu foams deposited at 1.8 A cm^{-2}

The average surface pore area varies between 108 μm^2 in Ni–Cu foams deposited at 60 s and 225 μm^2 for a deposition time of 180 s. If we consider that the surface pores are nearly circular these values correspond to average pore diameters between 12 and 17 μm for metallic foams deposited at 60 and 180 s, respectively. These results are in accordance with a previous report on Ni–Cu foams electrodeposited on copper-coated alumina substrates [15],

despite the difference in substrate material. This is attributed to the existence of a continuous layer at the foam/substrate interface and provides a full coverage of the substrate, so that the hydrogen bubbles will form at the dense layer and not on the substrate material itself. The interfacial continuous layer is likely to be formed during the early stages (first seconds) of deposition, preceding the formation of dendrites. The intensive hydrogen evolution changes the hydrodynamic conditions near the electrode and reduces the diffusion layer thickness. This hinders the diffusion control necessary for dendritic growth that is hence delayed, allowing at these early stages the formation of a continuous and dense layer.

As deposition progresses, and due to the high cathodic current applied, the agitation provided by hydrogen evolution is no longer sufficient to supply sufficient metal ions to be readily reduced at the substrate. Thus the deposition process becomes diffusion controlled and dendritic growth occurs.

The pores present in the Ni–Cu foams, as in Cu foams deposited by the same method, result from hydrogen bubble formation during the deposition process [6, 8, 9]. Therefore the morphology of the Ni–Cu foams is closely related to the nucleation and evolution of H_2 bubbles that occur simultaneously with the nucleation and growth the Ni–Cu agglomerates. Due to the high cathodic current applied, deposition of Ni and Cu occurs simultaneously with intense H_2 evolution, which is easily seen during deposition. Metal deposition occurs preferentially in the interstices between H_2 bubbles, forming metal grains. H_2 bubbles grow (or coalesce) with time and detach from the electrode, once a critical bubble size is reached. This creates regular shaped pores in the film, whose size increases with the distance to the substrate due to H_2 bubble coalescence. Furthermore, H_2 bubbles will also evolve at different locations and depths in the growing metallic foam, leading to a wide distribution of surface pores sizes.

A typical cross-section of a Ni–Cu foam is shown in Fig. 4. It can be confirmed that the stainless steel substrate is fully covered by a continuous layer of dense material, from which the dendritic structures evolve. A network of dendrites exists throughout the foam thickness and the dendrites themselves tend to decrease in size/thickness from the substrate/film interface upwards. Near the film surface, smaller/thinner dendrites are clearly observed. This has a beneficial effect on the foam stability, since the full structure is supported by both larger dendrites and a compact layer. Due to the cross-section preparation method, 3D pores are difficult to identify and the pore size along the cross-section could not be fully evaluated. However, it can be seen that near circular pores exist throughout the foam thickness and, as mentioned earlier, the pore walls are not compact, further contributing to the surface area enhancement.

Element distribution maps (Fig. 4c, d) show a composition gradient along the cross-section, evidencing that the Cu content in the film decreases continuously from the surface of the foam to the substrate film interface, in agreement with the work of Choi et al. [15]. These authors suggested that this effect can be related to the faster consumption of Ni ions comparatively to Cu ions, due to the formation of the Ni-rich phase around the substrate. However, in the present work, because of the higher Ni/Cu ratio used in the electrolyte solution, a more probable cause could be that as deposition progresses, the local active area at the surface of the deposit, where the metal nucleation and growth occurs, will decrease due to the formation dendrites and sharp protuberances at the film/electrolyte interface. Hence, at these sites, the potential required to achieve the imposed current density will became less negative, favouring the deposition of copper at the those sites.

The chemical composition of the electrodeposited Ni–Cu foams was determined by EDS and, as expected, the main elements detected were nickel and copper. Residual amounts (<2 at.%) of sulfur and chlorine were detected in some samples deposited for 180 s. The dependence of the average Ni–Cu atomic ratio in the films on the deposition time is shown in Fig. 5. The Ni content of the metallic foams decreases with deposition time and, for a deposition time of 180 s, only 61 at.% of Ni is detected in the deposit. Furthermore, the copper content in the foam is much higher than that in the deposition electrolyte. In solution, copper represents only 2 at.% of the metallic ions in solution but it reaches up to 40 at.% in metallic foams deposited for 180 s.

The standard reduction potential of copper (+0.337 V) is about 0.6 V less negative (more noble) than that of nickel (−0.25 V) [17]. This is actually the reason why most studies on the deposition of Ni–Cu alloys are performed on solutions containing copper complexing agents such as citrate, pyrophosphate and not simple metal solutions [18]. In the present work, during electrodeposition of Ni–Cu foams, Cu, being the most noble metal, deposits preferentially to Ni, explaining the reason why the content of Cu in the foam is higher than in solution. Accordingly, this process can be classified as preferential deposition as defined by Brenner [18].

It is generally accepted that the cathodic deposition of copper in acidic sulfate solutions occurs in two steps, the first one being the rate determining step [19]:

$$Cu^{2+} + e^- \rightarrow Cu^+, \quad E^0 = -0.087 \text{ vs. SCE} \tag{1}$$

$$Cu^+ + e^- \rightarrow Cu, \quad E^0 = 0.281 \text{ vs. SCE} \tag{2}$$

However, in the presence of chloride ions, the reduction of copper may occur according to reactions (1) and (2) or

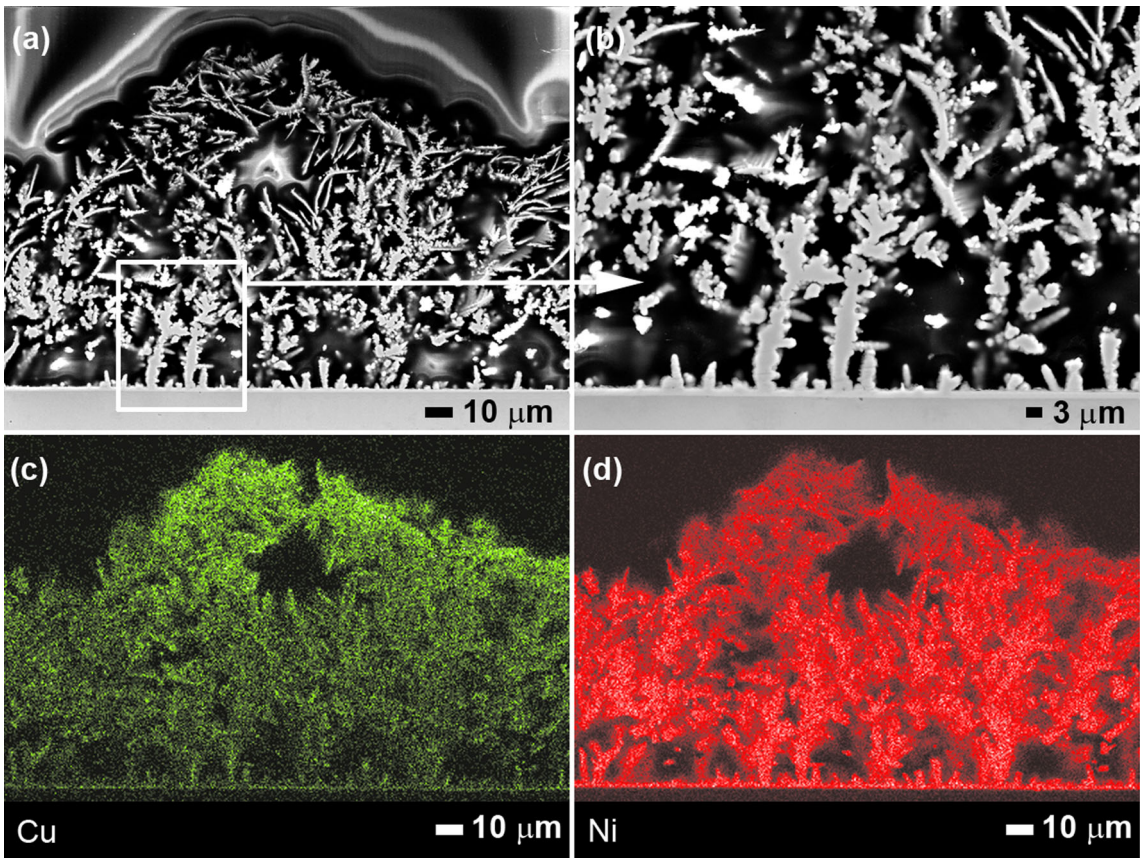

Fig. 4 SEM images (**a**, **b**) and element distribution maps of (**c**) Cu and (**d**) Ni the cross-section of Ni–Cu foam deposited at 1.8 A cm^{-2} for 180 s

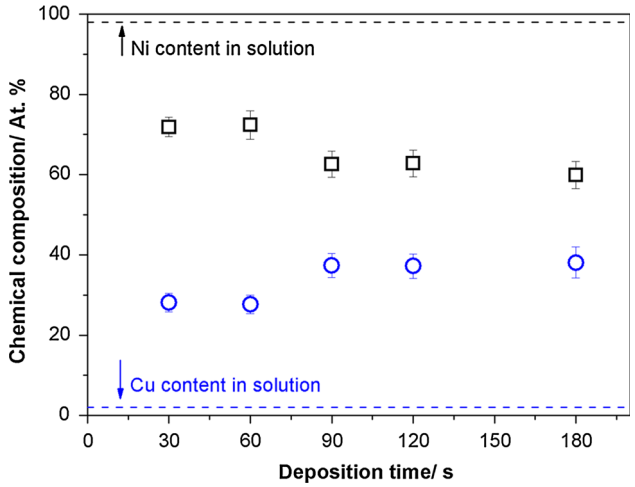

Fig. 5 Variation of Ni (*open square*) and Cu (*open circle*) atomic percentage in foams deposited at 1.8 A cm^{-2} with deposition time. *Horizontal lines* show the atomic percentage of Ni and Cu in the electrolytic solution

by a different 2-step reduction process involving the complexation of Cu^+ ions by Cl^- and adsorption of CuCl on the Cu surface [20, 21]:

$$Cu^+ + Cl^- \rightarrow CuCl_{ads} \quad (3)$$

$$CuCl_{ads} + e^- \rightarrow Cu + Cl^- \quad (4)$$

At high current densities, the second process becomes an efficient parallel path for Cu deposition, increasing the overall deposition rate of Cu [20, 21]. However, when the concentration of Cl^- ions is high (above 0.1 M) [22], the concentrations of free Cu^{2+} and free Cu^+ decrease due to the complexation of copper species and a cathodic polarization of the deposition process occurs.

Concerning, nickel electrodeposition it is generally accepted that it occurs in two consecutive steps and involves the formation of an intermediate complex adion (NiX_{ads}) [23, 24]:

$$Ni^{2+} + X^- \rightarrow NiX^+ \quad (5)$$

$$NiX^+ + e^- \rightarrow NiX_{ads} \quad (6)$$

$$NiX_{ads} + e^- \rightarrow Ni + X^- \quad (7)$$

If chloride is present in solution as in a Watts bath (formed of $NiSO_4$ + NaCl + H_3BO_3), the anion X should be Cl^- and the rate determining step the first electron transfer step (Eq. 5) [25].

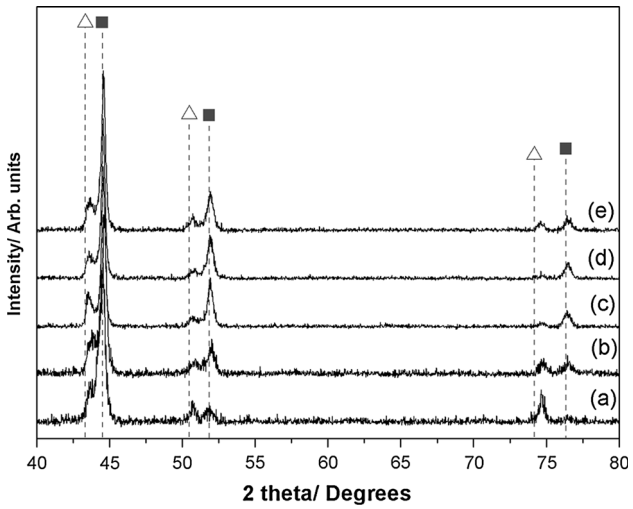

Fig. 6 X-ray diffractograms of Ni–Cu foams deposited at 1.8 A cm^{-2} for **a** 30, **b** 60, **c** 90, **d** 120 and **e** 180 s. *Vertical lines* represent diffraction peaks position for Cu, ICDD 01-070-3039 (*open triangle*) and nickel ICDD 00-04-0850 (*filled square*)

On the other hand, the pH of the solution also influences the deposition processes. In sulfate-based electrolytes the pH decrease from 3 to 1 leads to a decrease of the overpotential for Ni deposition [26].

The effects described above suggest that the highly acidic electrolyte used in the present work could promote Ni deposition, while the presence of excess Cl^- could act as an inhibitor for Cu deposition. In fact, the dense layer formed at the substrate/film interface does have a high percentage of nickel, suggesting that during the early stages of deposition, nickel is preferentially deposited over copper. However, and as deposition progresses, copper deposition is favoured giving rise to a concentration gradient throughout the thickness of the foam.

X-ray diffractograms of Ni–Cu foams depict several diffraction peaks (Fig. 6), indicating a crystalline nature. Nickel and copper have a full mutual solubility as predicted by the respective phase diagram [27] and it is well known that Ni–Cu alloys for solid solutions with face centred cubic (fcc) structure. All diffractograms present multiple peaks. The peaks at ~44.6°, 51.9°, and 76.5° are nearly coincident with (111), (200) and (220) reflections of fcc nickel (ICDD 00-04-0850), respectively, presenting a slight shift to higher 2θ angles. The peaks at 43.7°, 50.8°, 74.7° are closer to the position of fcc copper (ICDD 01-070-3039), presenting a shift to higher 2θ angles.

Table 1 shows the average lattice parameter (*a*) value of the phases present in Ni–Cu foams calculated from the XRD data presented in Fig. 6. Ni–Cu alloys follow Veggard's law that claims a linear relationship between lattice parameter and alloy composition [16]. Hence, even 1 % of Cu in solid solution with Ni would promote an increase of the respective lattice parameter in relation to fcc nickel

Table 1 Lattice parameter (a) calculated from XRD data shown in Fig. 6

Deposition time (s)	Average a (Å)	
	Ni-phase	Cu-phase
30	3.522	3.590
60	3.516	3.592
90	3.519	3.593
120	3.518	3.592
180	3.519	3.594

($a = 3.5239$ Å, ICDD 00-04-0850). However, the average *a* values calculated for the Ni-phase (Table 1) do not show an increase in relation to pure fcc nickel which indicates the presence of a pure nickel phase in the deposited foams.

The average *a* values calculated for the copper phase (Table 1) are lower than fcc copper ($a = 3.6148$ Å, ICDD 01-070-3039) suggesting the presence of Ni in solid solution. It is important to refer that although the copper content in the films increases with the deposition time, the lattice parameters of its crystalline phases does not change significantly, indicating that the phases remain the same as deposition time increases. It should be noted that no pure copper phase was detected in the diffractograms. According to Veggard's law, the copper-rich should have ~25 % of nickel in solid solution.

The electrochemical behaviour of Ni–Cu foams was evaluated in 1 M KOH solution by cyclic voltammetry and chronopotentiometry. Representative cyclic voltammograms of Ni–Cu foams (Fig. 7) are distinct from voltammograms of materials exhibiting an electric double layer charge storage mechanism [28], presenting oxidation and reduction peaks that indicate a pseudocapacitive behaviour, i.e., charge storage originates from reversible redox reactions. The voltammograms of Ni–Cu foams have a couple redox peaks in the potential range of −0.2 to +0.8 V. The anodic peak is related to the oxidation of $Ni(OH)_2$ to a higher-valence oxy-hydroxide (NiOOH), while the cathodic peak is associated to the corresponding reduction reaction, following the equation [29]:

$$Ni(OH)_2 + OH^- \leftrightarrow NiOOH + H_2O + e^- \quad (8)$$

Although the Ni–Cu foams were not submitted to oxidation pre-treatments, their voltammetric response is in accordance with that reported in the literature for Ni oxides in alkaline solutions [30], suggesting that the Ni–Cu foam is oxidised upon its immersion on the KOH solution and potential cycling. In this potential range, copper undergoes one redox reaction Cu(II)/Cu(III) involving CuO surface species [31]. However the corresponding voltammetric wave is not detected in the voltammetric curves, which can be explained by the fact that in Cu–Ni alloys copper

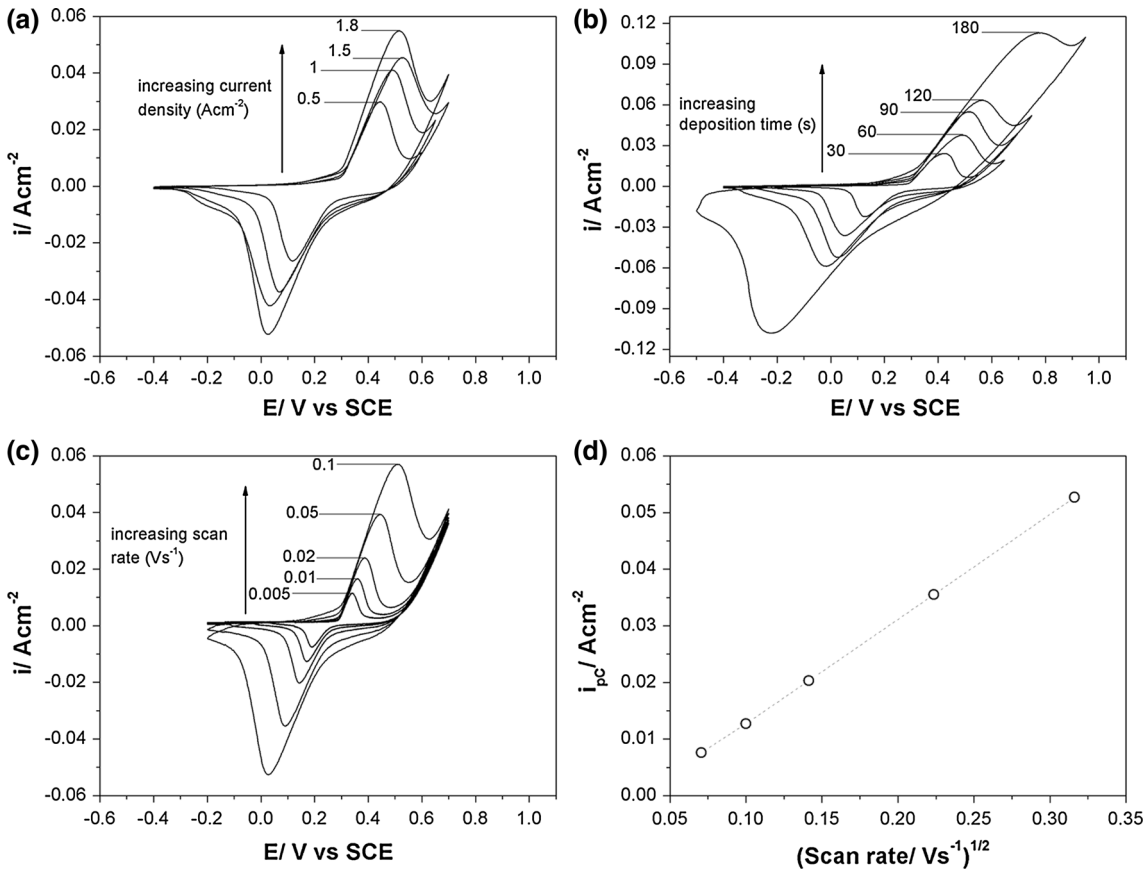

Fig. 7 Cyclic voltammograms of 1 M KOH solution on Ni–Cu foams **a** deposited during 90 s at different current densities (scan rate 100 mV s^{-1}), **b** deposited at 1.8 A cm^{-2} with different deposition times (scan rate 100 mV s^{-1}), **c** deposited at 1.8 A cm^{-2} for 90 s with increasing scan rates and **d** the variation of the cathodic peak current with the square root of the scan rate

oxidation reactions are hindered due to the formation of a protective nickel hydroxide film [32].

Both the increase of applied current density and the deposition time lead to an increase of the current density and total charge measured by cyclic voltammetry (Fig. 7a, b), having a beneficial effect on the electrochemical activity of the films.

The influence of the potential scan rate on the voltammetric response of Ni–Cu foam deposited at 1.8 A cm^{-2} for 90 s is presented in Fig. 7c. The magnitude of the current density of the cathodic peak (ip_C) varies linearly with the square root of the scan rate (υ) (Fig. 7d), indicating that the deposition process is diffusion controlled. On the other hand, the potentials corresponding to the anodic and cathodic peaks vary with υ (Fig. 7c) and the peak separation is larger than that for reversible reactions (0.059 V at 298 K) [33] which indicates that the redox reaction is not totally reversible.

It is also observed that as the deposition time increases, there is an increase of peak separation along with broadening of the peaks observed in the voltammograms (Fig. 7b). This effect is still not clearly understood. High peak separation in the cyclic voltammograms of porous materials has been attributed to both ohmic resistance due to the electrolyte diffusion through the pores and polarization of the electrode material [34]. In Fig. 7 it can be seen that peak separation tends to increase with the deposition time and the applied current, suggesting that this behavior is related to the electrolyte diffusion throughout the volume of the foam that increases with both deposition time and applied current, due to the formation of a more interconnected 3D structure. Furthermore, one should keep in mind that the porosity of the Ni–Cu foams may affect their voltammetric response. As stated previously, peak separation is a common criterion of the reversibility of electron transfer but this is valid if a semi-infinite diffusion to a flat electrode is assumed. When comparing the voltammograms in Fig. 7b it is worth to consider that the foams present different active areas/porosity, so that the mass transport mechanism is probably not the same for all of them. Menshykau and Compton [35] have reported that the electrode porosity and morphology can significantly affect the voltammograms shape, in particular peak current and separation, since in porous electrodes a thin layer

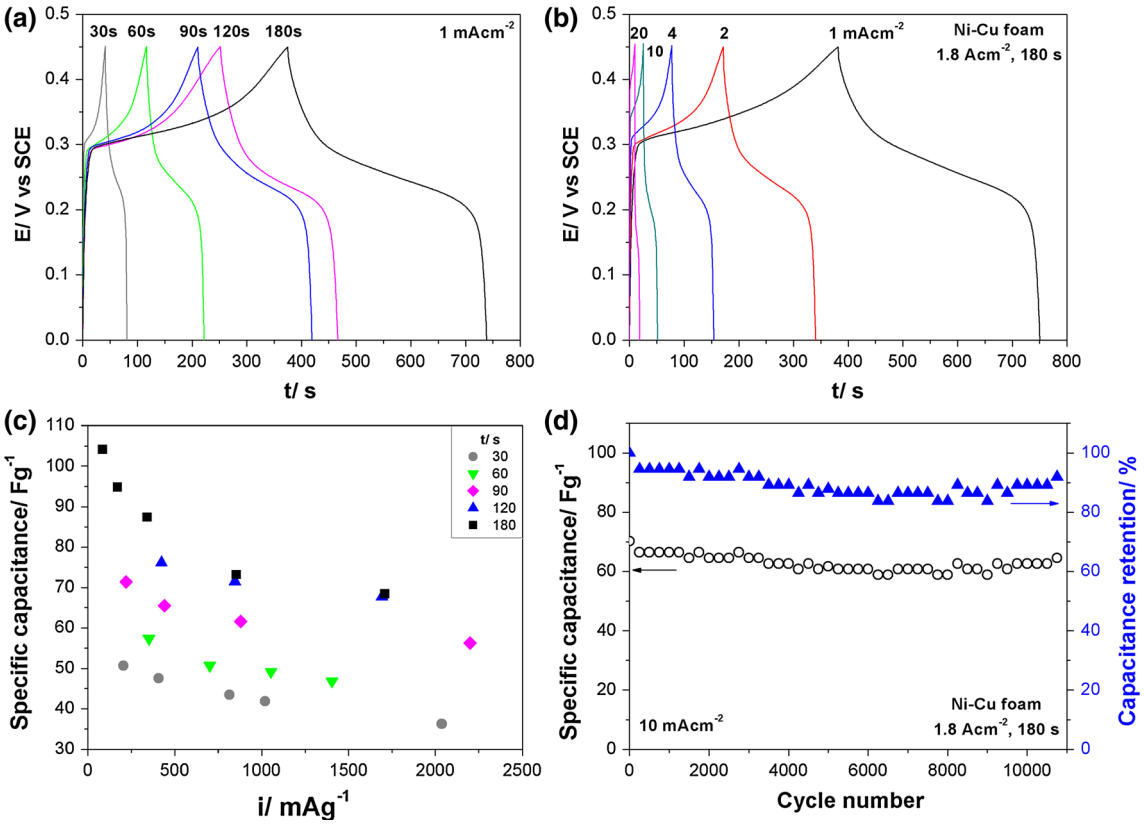

Fig. 8 Galvanostatic charge–discharge curves of Ni–Cu foams: **a** effect of deposition time and **b** effect of applied charge–discharge current; **c** variation of specific capacitance with applied charge–discharge current and the deposition time and **d** cycling stability of Ni–Cu foams deposited at 1.8 A cm^{-2} during 180 s at 10 mA cm^{-2}

diffusion regime may occur. Finally, the differences observed in the voltammograms could also be related to changes in the chemical composition of the Ni–Cu foams with the deposition time, since the copper content increases with the deposition time (Fig. 5). However, this hypothesis seems unlikely because the redox reactions occurring at the potential rate of the voltammograms are due to the nickel phase, so that variations of the copper content are not expected to affect the reaction occurring at that potential.

The galvanostatic charge–discharge curves of Ni–Cu foams deposited at 1.8 A cm^{-2} are presented in Fig. 8a, b. As expected, the curves are not triangular in shape and present charge and discharge plateaus, resulting from the redox reactions that occur in this potential range. This confirms the pseudocapacitance behaviour of the Ni–Cu in agreement with the cyclic voltammetry results. The specific capacitance of the Ni–Cu foams was calculated from charge–discharge data using the equation [28]:

$$C = \frac{i\Delta t}{m\Delta V} \tag{9}$$

where i is the applied current density, Δt is the discharge time, m is the mass of active material and ΔV is the potential window. The variation of specific capacitance with the deposition time is presented in Fig. 8c. Ni–Cu foams deposited for 180 s presented the highest specific capacitance value, 105 F g^{-1} at 1 mA cm^{-2}, maintaining 75 % of capacitance when the charge/discharge rate is changed from 1 to 10 mA cm^{-2}. The higher capacitance of Ni–Cu foams deposited with longer deposition times may be explained by the higher number of accessible electroactive surface sites for redox reactions (higher surface area).

Long term cycling stability is an important characteristic of supercapacitor electrode materials, which is evaluated by consecutive charge–discharge measurements. After 10,000 cycles at 10 mA cm^{-2}, the Ni–Cu foams present a capacitance retention of approximately 90 %, showing therefore an excellent cyclic stability, better than previous reports on nanoporous nickel oxides and hydroxides [34, 36].

It should be noted that the capacitance values of the Ni–Cu foams are much lower than those reported in the literature for Ni oxide/hydroxide materials [1]. This can be explained by the fact that the Ni–Cu NMFs have not suffered any oxidation treatment prior to testing so that the active material (Ni oxides/hydroxides) is formed only as a

superficial layer, accounting for a small fraction of the deposited mass, for which the specific capacitance was calculated. Thermal conditioning of the Ni–Cu foams could therefore increase the amount of Ni oxides/hydroxides in the films and contribute to an increase of the capacitance value. Additionally, the addition of other elements with multiple oxidation states such as cobalt or manganese could also improve the performance of the Ni–Cu foams due to the synergetic effect between the different elements. Both strategies are currently being developed and will be presented in future reports.

4 Conclusions

Cathodic electrodeposition coupled with the dynamic hydrogen bubble template has been used for the fabrication of nanostructured metallic foams. Porous Ni–Cu metallic foams, with randomly distributed nearly-circular pores, whose walls have of an open dendritic structure, have been tailored on stainless steel substrates by controlling for applied current densities above 1 A cm^{-2}. The Ni–Cu metallic foams have copper content much higher than that in the electrolyte solution and they are composed of pure nickel and a copper-rich phase containing nickel in solid solution.

The Ni–Cu foams present a pseudocapacitive behaviour, charge storage arising from reversible redox reactions of the nickel phase. A maximum specific capacitance value of 105 F g^{-1} at 1 mA cm^{-2} was obtained for foams deposited at 1.8 A cm^{-2} during 180 s. The cyclic stability of these materials is high and they present a capacitance retention of 90 % after 10,000 cycling tests.

Acknowledgments The authors would like to acknowledge financial support from Fundação para a Ciência e Tecnologia (FCT) under the project PTDC/CTM-MET/119411/2010 "Electrodeposition of oxide spinel films on stainless steel substrates for the development of new electrodes for supercapacitors", COST Action MP1004-"Hybrid Energy Storage Devices and Systems for Mobile and Stationary Applications" and COST Action MP1106-"Smart and green interfaces—from single bubbles and drops to industrial, environmental and biomedical applications"

References

1. Wang G, Zhang L, Zhang J (2012) A review of electrode materials for electrochemical supercapacitors. Chem Soc Rev 41(2): 797–828
2. Tappan BC, Steiner SA, Luther EP (2010) Nanoporous metal foams. Angew Chem Int Ed 49(27):4544–4565
3. Erlebacher J et al (2001) Evolution of nanoporosity in dealloying. Nature 410:450–453
4. Silva RP et al (2012) Fabrication of three-dimensional dendritic Ni–Co films by electrodeposition on stainless steel substrates. J Phys Chem C 116(42):22425–22431
5. Nikolić ND et al (2006) Morphologies of copper deposits obtained by the electrodeposition at high overpotentials. Surf Coat Technol 201:560–566
6. Shin H-C, Liu M (2004) Copper foam structures with highly porous nanostructured walls. Chem Mater 16:5460–5464
7. Shin HC, Dong J, Liu M (2003) Nanoporous structures prepared by an electrochemical deposition process. Adv Mater 15:1610–1614
8. Nikolić N (2010) Fundamental aspects of copper electrodeposition in the hydrogen co-deposition range. Zaštita materijala 51:197–203
9. Nikolić ND et al (2006) Phenomenology of a formation of a honeycomb-like structure during copper electrodeposition. J Solid State Electrochem 11:667–675
10. Tan K, Tian M-B, Cai Q (2010) Effect of bromide ions and polyethylene glycol on morphological control of electrodeposited copper foam. Thin Solid Films 518:5159–5163
11. Nam D et al (2011) Effects of $(NH_4)_2SO_4$ and BTA on the nanostructure of copper foam prepared by electrodeposition. Electrochim Acta 56:9397–9405
12. Cherevko S, Xing X, Chung C-H (2010) Electrodeposition of three-dimensional porous silver foams. Electrochem Commun 12:467–470
13. Yang G-M et al (2011) Bubble dynamic templated deposition of three-dimensional palladium nanostructure catalysts: approach to oxygen reduction using macro-, micro-, and nano-architectures on electrode surfaces. Electrochim Acta 56:6771–6778
14. Cherevko S, Chung C-H (2011) Direct electrodeposition of nanoporous gold with controlled multimodal pore size distribution. Electrochem Commun 13(1):16–19
15. Choi W-S et al (2012) Nanostructured metallic foam electrodeposits on a nonconductive substrate. J Mater Chem 22:1028–1032
16. Cullity BD (1978) Elements of X-ray diffraction. Addison-Wesley Publishing Company, Boston
17. Pourbaix M (1974) Atlas of electrochemical equilibria, 2nd edn. National Association of Corrosion Engineers, Houston
18. Brenner A (1963) Electrodeposition of alloys principles and practice. Academic Press, San Diego
19. Mattsson E, Bockris JM (1959) Galvanostatic studies of the kinetics of deposition and dissolution in the copper + copper sulphate system. Trans Faraday Soc 55:1586–1601
20. Gabrielli C et al (2004) Mechanism of copper deposition in a sulphate bath containing chlorides. J Electroanal Chem 572:367–375
21. Soares DM et al (2002) Copper ion reduction catalyzed by chloride ions. J Electroanal Chem 532:353–358
22. Shao W, Pattanaik G, Zangari G (2007) Influence of chloride anions on the mechanism of copper electrodeposition from acidic sulfate electrolytes. J Electrochem Soc 154:D201–D207
23. Epelboin I, Joussellin M, Wiart R (1981) Impedance measurements for nickel deposition in sulfate and chloride electrolytes. J Electroanal Chem 119:61–71
24. Oriňáková R et al (2006) Recent developments in the electrodeposition of nickel and some nickel-based alloys. J Appl Electrochem 36:957–972
25. Saraby-Reintjes A, Fleischmann M (1984) Kinetics of electrodeposition of nickel from watts baths. Electrochim Acta 29(4): 557–566
26. Santana AIC et al (2009) A kinetic study on nickel electrodeposition from sulfate acid solutions. J Electrochem Soc 156:D326–D330
27. Chakrabarti DJ et al (1992) Cu–Ni (copper–nickel) phase diagram. In: Metals handbook, vol. 3: alloy phase diagrams. ASM International, Russel
28. Conway BE (1999) Electrochemical supercapacitors: scientific fundamentals and technological applications. Kluwer Academic, New York
29. Yau S-L et al (1994) In situ scanning tunneling microscopy of Ni (100) in 1 M NaOH. J Phys Chem 98(21):5493–5499

30. Hu C–C, Chang K-H, Hsu T-Y (2008) The synergistic influences of OH^- concentration and electrolyte conductivity on the redox behavior of $Ni(OH)_2$/NiOOH. J Electrochem Soc 155(8):F196–F200
31. Medina AMCLd, Marciano SL, Arvia AJ (1978) The potentiodynamic behaviour of copper in NaOH solutions. J Appl Electrochem 8:121–134
32. Ismail K, Fathi A, Badawy W (2004) The influence of Ni content on the stability of copper–nickel alloys in alkaline sulphate solutions. J Appl Electrochem 34(8):823–831
33. Bard AJ, Faulkner LR (2001) Electrochemical methods fundamentals and applications. Wiley, New York
34. Meher SK, Justin P, Ranga Rao G (2011) Nanoscale morphology dependent pseudocapacitance of NiO. Influence of intercalating anions during synthesis. Nanoscale 3(2):683–692
35. Menshykau D, Compton RG (2008) The influence of electrode porosity on diffusional cyclic voltammetry. Electroanalysis 20(22):2387–2394
36. Wu M-S et al (2007) Electrodeposition of nanoporous nickel oxide film for electrochemical capacitors. Int J Hydrogen Energy 32(17):4153–4159